Talanta 146 (2016) 291–298

Contents lists available at ScienceDirect

Talanta

journal homepage: www.elsevier.com/locate/talanta

Self-referencing fiber optic particle plasmon resonance sensing system for real-time biological monitoring

Chin-Wei Wu [a], Chang-Yue Chiang [a,b], Chien-Hsing Chen [b], Chung-Sheng Chiang [b], Chih-To Wang [b], Lai-Kwan Chau [a,b,*]

[a] Department of Chemistry and Biochemistry, National Chung Cheng University, Chiayi 62102, Taiwan
[b] Center for Nano Bio-Detection (AIM-HI), National Chung Cheng University, Chiayi 62102, Taiwan

ARTICLE INFO

Article history:
Received 5 July 2015
Received in revised form
23 August 2015
Accepted 24 August 2015
Available online 29 August 2015

Keywords:
Biosensor
Fiber optic sensor
Self-referencing
Particle plasmon resonance
Gold nanoparticle

ABSTRACT

We present the design and experimental verification of a self-referencing dual-channel fiber optic particle plasmon resonance (FOPPR) sensing system for compensation of thermal and bulk-composition effects as well as nonspecific adsorption in real-time biosensing of complex samples. A theoretical model is first proposed and then a systematic experimental approach is used to verify the model. The sensing system comprises an analysis fiber sensor and a reference fiber sensor in a single microfluidic chip, where the analysis fiber is functionalized with a recognition molecule. The compensation still works even if the surface coverages of gold nanoparticles on the reference and analysis fibers are not exactly the same. The potential of this approach is illustrated by a model biosensing experiment in which the detection of anti-biotin is compensated for bulk refractive index change, nonspecific adsorption and/or color interference, in various sample media. The percent recovery is 103.2% under both the effects of bulk refractive index change and nonspecific adsorption and is 93.9% under both the effects of color interference and nonspecific adsorption, suggesting that the compensation is effective.

1. Introduction

One of the concerns for many label-free optical biosensors [1–3], such as those based on surface plasmon resonance (SPR), particle plasmon resonance (PPR), interferometer, waveguide, ring resonator, and photonic crystal, is that the detected signal is not totally due to the specific binding of the analyte but also include systematic errors such as temperature fluctuation, bulk refractive index change, color interference, and/or nonspecific adsorption [4–7]. In many cases, the detected signals often have a magnitude similar or lower than the systematic errors. Thus, it is necessary to accurately separate or compensate the systematic errors in order to produce meaningful data. Such systematic errors are typically corrected through the use of a reference sensor that is monitored in parallel with the analysis sensor [4,6,7].

Recently, biosensors based on particle plasmon resonance (PPR), also known as localized surface plasmon resonance (LSPR), have received more and more attention because of the high sensitivity of the PPR spectrum of noble metal nanoparticles to adsorbate-induced changes in the local refractive index (RI) of the surrounding environment [3,8–10]. For biosensor applications, gold nanoparticles (AuNPs) are particularly attractive because of its chemical stability, simple and reproducible preparation procedures, and convenient spectral window in the visible region. When an analyte binds with a corresponding recognition molecule on the AuNP surface, an increase of the plasmon absorbance and a shift of the plasmon peak wavelength will result [11–13]. The plasmon absorbance-based PPR biosensing system is especially attractive because it employs a simple extinction measurement which just requires a simple optical configuration without using a bulky and expensive spectrophotometer [14,15]. Despite the advantages of the plasmon absorbance-based PPR biosensing method, the issue of the low absorbance of a AuNP submonolayer obtained by either the transmission mode with a single pass of light or reflection mode with a double pass of light needs to be solved to enhance the sensitivity of detection [12,13].

To overcome the above limitation, we have developed a label-free and real-time fiber optic particle plasmon resonance (FOPPR) sensor, which is based on gold nanoparticles-modified optical fiber [16–19]. This sensor utilizes the evanescent wave via the consecutive total internal reflection (TIR) scheme in an optical fiber to increase the absorbance of a submonolayer of AuNPs on the core surface [18,20]. Thus it significantly enhances the signal-to-noise (S/N) ratio achieved by the AuNP submonolayer sensing structure, offering advantages like label-free, real-time, high biosensing

* Corresponding author at: Department of Chemistry and Biochemistry, National Chung Cheng University, Chiayi 62102, Taiwan. Fax: +886 5 2721040.
E-mail address: chelkc@ccu.edu.tw (L.-K. Chau).

http://dx.doi.org/10.1016/j.talanta.2015.08.047
0039-9140/

sensitivity (nM–pM), wide linear dynamic range, easy-to-operate, normalized sensor response, ease-of-multiplexing, ease-of-miniaturization, low-cost optical configuration, and easy fabrication of inexpensive sensor elements [5,19,21–24]. The FOPPR biosensor has been applied to quantitative measurement of antinuclear antibodies in sera [14], cytokines and matrix metalloproteinases in synovial fluids [19,23], and orchid viruses in leaf saps [5], with results agree quantitatively with the clinically accepted enzyme-linked immunosorbent assay (ELISA) method.

Since the FOPPR biosensor measures changes in local refractive index surrounding the AuNPs, excessive dilution of real samples are often needed in order to match the RI of the sample with the blank. As a result, the limit of detection (LOD) is compromised. In other cases, when using high RI solvents such as DMSO, glycerol, and ethanol, the variability of the solvent content from one sample to another will result in a measurement variability that is due solely to the RI of the sample. Furthermore, many kinds of real samples like plant saps and whole blood have a color overlapping with the excitation spectrum of the incident light. As a result, spectral interference will occur and lead to systematic error in the analysis [5]. Although using nanostructures with the PPR band in the near-infrared region, such as gold nanorod [5] and gold nanoshell [25], may avoid the color interference problem. Preparation of such anisotropic nanoparticles in a simple and reproducible manner is still very challenging.

In this work, we start from a theoretical model and follow by a systematic experimental verification approach to demonstrate a method for highly accurate compensation of systematic errors such as temperature fluctuation, bulk refractive index change, color interference, and/or nonspecific adsorption by using a self-referencing dual-channel FOPPR sensing system which comprises an analysis fiber and a reference fiber in a single microfluidic chip. The dual-channel system maintains the advantages of the single-channel FOPPR sensing system and further provides the capability of detecting low concentration of analytes in complex samples without excessive dilution. Moreover, the system can compensate the light source fluctuation and the effects from surrounding environment (e.g., temperature, vibration, and so on). Hence, it is potentially applicable to environmental, agricultural, food, and clinical analysis.

2. Materials and methods

2.1. Reagents and materials

Hydrogen tetrachloroaurate trihydrate ($HAuCl_4$), 11-mercaptoundecanoic acid (MUA), 6-mercapto-1-hexanol (MCH), N-hydroxy-succinimide (NHS), and carbodiimine hydrochloride (EDC), bovine serum albumin (BSA), N-(+)-biotinyl-3-aminopropylammonium trifluoroacetate, and anti-biotin antibody were purchased from Sigma-Aldrich. (3-Mercaptopropyl)-methyl-dimethoxy silane (MPDMS) and erythrosine were purchased from Tokyo Chemical Industry Co. Trisodium citrate was purchased from Showa Chemical Industry Co. Phosphate buffered saline (PBS) powder was from Zeus Scientific, Inc. Ultrapure water (18.2 MΩ cm) were purified by Milli-Q water system (Millipore) and used to prepare all aqueous solutions. Solutions of various refractive indexes (1.33387–1.35726) were prepared by dissolving PBS powder with water to be a solution first and then further diluted with a dilution ratio between 1 time and 20 times. The RI of the solutions was measured by a refractometer (RA-620, Kyoto Electronics).

2.2. Preparation of sensor fibers

The optical fibers used as the FOPPR sensor fibers are multimode plastic-clad silica fiber (model F-MBC, Newport) with core and cladding diameters of 400 and 430 μm, respectively. A segment of 20 mm of the coating and cladding in the middle section of the optical fibers was removed by using a CO_2 laser processing system (V-460, Universal Laser Systems Inc.) to form a sensing window [26]. The fiber end faces were polished to an optically smooth surface to increase the transmission efficiency. Such partially unclad fibers after modification with AuNPs were used as the FOPPR sensor fibers.

AuNPs were synthesized accordance to the previous procedure [20] with slight modification. A $HAuCl_4$ solution (0.88 mM, 50 mL) was heated to boiling with vigorous stirring for about 15 min. Then a fresh trisodium citrate solution (1%, 6 mL) was rapidly added in the boiling solution. The solution was kept boiling for 10 min and the color changed from yellow to ruby-red. The resulting solution was allowed to cool down to room temperature while kept stirring for 10 min. The spectrum of the AuNP solution was obtained by a double beam UV-Visible spectrometer (Cintra 202, GBC). The peak wavelength of the AuNP solution was at about 519 nm. The images of the AuNPs were obtained by a transmission election microscope (TEM, JEOL 1200 EX). By TEM image analysis, the diameter of the AuNPs is 13.5 ± 1.1 nm.

Using the partially unclad fibers, AuNPs were anchored on the sensing window as shown in Fig. 1A. Before anchoring of AuNPs on the sensing window, the optical fibers were cleaned by a mixture of H_2SO_4 and H_2O_2 with volume ratio of 3:2. After cleaning, the optical fibers were immersed in a mixture of MPDMS and toluene (volume ratio = 1:49) for 4 h to functionalize the sensing window with thiol group. The mixture of MPDMS and toluene was pre-hydrolyzed overnight before use. After rinsing, the optical fibers were immersed in an AuNP solution for 2 h to allow the AuNPs to self-assemble on the sensing window of the optical fibers.

Using the AuNP-modified optical fibers, the analysis fiber and reference fiber were prepared via two different routes as shown in Fig. 1B. The AuNP surface of both the analysis and reference fibers was first modified with a mixed self-assembled monolayer (SAM) of MUA/MCH by immersing the AuNP-modified optical fibers in an ethanolic solution of MUA (0.4 mM) and MCH (1.6 mM) overnight at ambient temperature. Then, the carboxyl group of the mixed SAM was activated by immersing the fibers in an aqueous solution of EDC (0.2 M) and NHS (0.05 M) for 2 h. To prepare the analysis fiber for anti-biotin, the activated carboxyl group on the fibers was allowed to react with N-(+)-biotinyl-3-aminopropylammonium trifluoroacetate (10 μM) for 2 h. To prepare the reference fibers, the activated carboxyl group on the fibers was allowed to react with BSA (10 μM) for 2 h. The nonreacted carboxyl group was then deactivated by immersing the fibers in ethanolamine (1 M) for 30 min.

2.3. Microfluidic chip fabrication

The microfluidic sensor chip was composed of two FOPPR sensor fibers and two polycarbonate (PC) plates. The PC plates were produced by injection molding techniques. The cover plate had three holes to connect tubing (one inlet and two outlets) and the bottom plate had two microchannels with a depth of 900 μm and a width of 900 μm, as shown in Fig. 2, to place the two optical fibers. The dimensions of the plates are 25 mm (width) × 35 mm (length) × 2 mm (thickness). The cover and bottom plates were stuck together by a 3M double-sided bonding tape to assemble the chip. The free volume of the microchannels in the chip was about 43 μL.

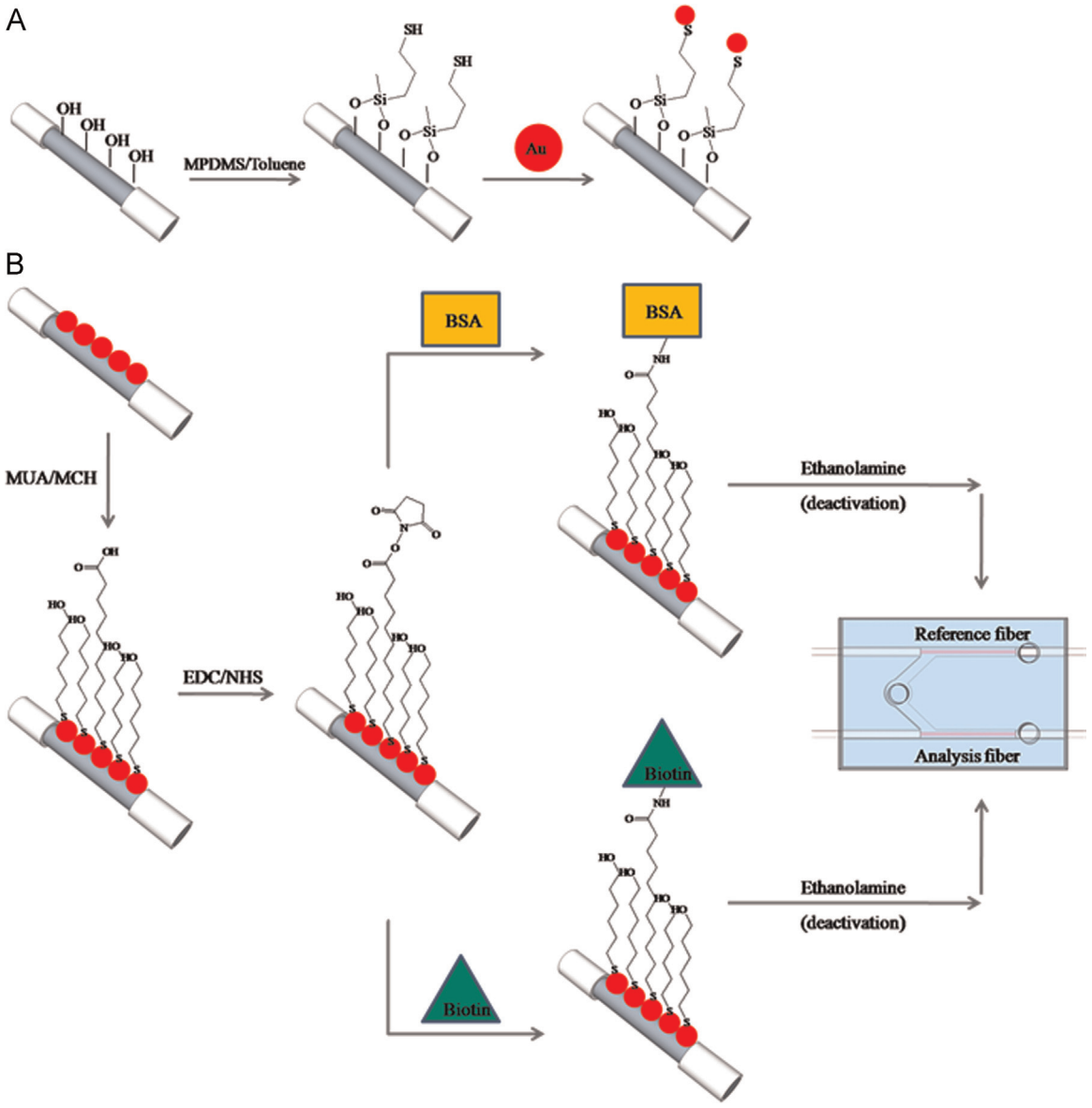

Fig. 1. (A) A schematic of anchoring AuNPs on the sensing window of a partially unclad optical fiber. (B) A schematic of preparation of analysis fiber and reference fiber using the AnNP-modified optical fiber in Fig. 1A.

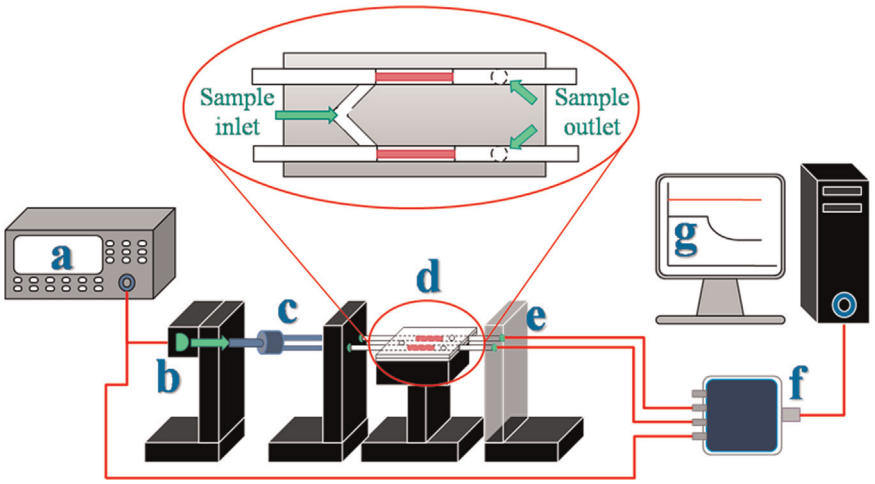

Fig. 2. A schematic of the self-referencing dual-channel FOPPR sensing system which consists of (a) function generator, (b) LED, (c) 1 × 2 optical fiber coupler, (d) sensor chip, (e) photodiode, (f) data acquisition card, and (g) computer.

2.4. Self-referencing dual-channel FOPPR sensing system

A schematic of the self-referencing dual-channel FOPPR sensing system is shown in Fig. 2. A function generator (SFG-2007, GW Instek) drives a light-emitting diode (LED, 530 nm, HPF8b-43K3GA/WPCB, HUEY-JANN Electronics) with 1 kHz frequency. The incident light from the LED enters the proximal ends of the two optical fibers in the sensor chip through a 1×2 optical fiber coupler (QBIF400-UV-VIS, Ocean Optics). Then the light beams exiting the distal ends of the two optical fibers were collected by two photoreceivers (S1336-18BK, Hamamatsu). The responses of the two photoreceivers are digitized by a 24-bit analog to digital converter (USB-9234, National Instruments), which has a maximum signal-to-noise ratio (SNR) $= 20 \times \log(2^{24}) = 144$ dB [27,28], and analyzed by custom software written in LabVIEW (National Instruments). The software provides continuous monitoring and analysis of the sensorgrams, calculates statistical noises in the system, and displays sensor responses versus time.

3. Result and discussion

3.1. Principle of self-referencing in dual-channel FOPPR sensing system

The FOPPR sensing technique is based on the absorption of evanescent wave by an AuNP layer on the core surface of an optical fiber. When light propagates along the optical fiber by consecutive TIRs, the AuNPs are excited by the evanescent field and thus the light transmitted through the fiber is attenuated by interaction with the AuNPs. As the attenuation is enhanced by multiple TIRs, the low absorbance of the AuNP layer can be significantly enhanced [18,20]. If P_{in} is the optical intensity of the incident light into the fiber, P_{out} is the optical intensity of the transmitted light through the partially unclad fiber in a liquid environment of various refractive indexes. For reasonably strong attenuating sensor, the fraction of guided power contained in the evanescent fields of all the fiber modes launched is given as [29,30]:

$$\frac{P_{out}}{P_{in}} = \frac{2\pi\rho(n_1^2 - n_2^2)^{1/2}}{\alpha L\lambda}$$

where ρ is the radius of the fiber core, n_1 is the refractive index of the fiber core and n_2 is the refractive index of the sensing medium, α is the absorption coefficient of the AuNP layer, L is the sensing length, and λ is the wavelength of the light source. Take an example in one of our cases, $n_1 = 1.51$, $n_2 = 1.333$, $\rho = 200$ μm, $\lambda = 0.530$ μm, and $\alpha = 1.97 \times 10^3$ cm^{-1}, where $\alpha = \varepsilon C$ is estimated by assuming an AuNP layer comprising of 13 nm AuNPs with a molar extinction coefficient (ε) of 2.47×10^8 M^{-1} cm^{-1} [31] and having a surface coverage of 0.2 whereas the AuNP concentration (C) is calculated by supposing the AuNPs in the AuNP layer were dispersed within an average penetration depth of the evanescent wave [32]. Thus, in a multimode fiber with many thousands of modes, the fraction of guided power carried into the sensing surface of the partially unclad fiber is roughly estimated to be about 42.7%. Details of the theoretical model and analysis are beyond the scope of this paper and will be reported elsewhere.

Because this PPR sensing technique is based on the absorbance change of the AuNP layer at different RI environments, we assume the absorption coefficient of the AuNP layer will increase from α_0 in a blank to $\alpha_0 + \Delta\alpha$ in a sample when the medium RI surrounding the AuNP layer increases by Δn [19]. Hence, if we plot $\Delta\alpha/\alpha_0$ versus Δn, a linear regression line with a calibration slope m will be obtained. Since the FOPPR sensor response can be approximated by the following relationship [19]:

$$\Delta I/I_0 = (I_0 - I)/I_0 = 1 - I/I_0 \approx \Delta\alpha/\alpha_0$$

where the normalized response, $\Delta I/I_0$, is defined as the collected signal intensity from an AuNP-modified optical fiber immersed in a sample (I) to that of the same fiber immersed in a blank (I_0), a plot of $\Delta I/I_0$ versus Δn will also yield a linear regression line with a calibration slope m. Since molecular binding on the AuNP surface will induce an increase of local RI within the sensing depth of the AuNP [30], the binding will result in a decrease in transmitted light intensity exiting the optical fiber. Therefore, with a recognition molecule conjugated on the AuNP surface, a corresponding analyte can be detected in real-time without the use of a label.

Thermal and bulk-composition effects can generate significant changes in the FOPPR sensor response, which may obscure those caused by specific binding of the analyte. In this study, we use a self-referencing mechanism in a dual-channel FOPPR sensing system to compensate those effects (thermal, bulk refractive index, and color interferences) in complex samples. The first optical fiber, the analysis fiber sensor with immobilization of a specific recognition molecule, will measure specific binding of an analyte as well as undesirable thermal and bulk-composition effects. Ideally, there should be no nonspecific adsorption at the analysis fiber. However, in reality, nonspecific adsorption is difficult to be avoided completely. As such, the compensated response can be described by the following relationship:

$$\frac{\Delta I_S}{I_{S0}} = m_S \times (\Delta n_M + \Delta n_{NA} + \Delta n_{SA}) \quad (1)$$

where $\Delta I_S/I_{S0}$ is the normalized response of the analysis fiber, m_s is the calibration slope of the analysis fiber, Δn_M is the change of bulk RI of the medium, Δn_{NA} is the change of effective local RI due to nonspecific adsorption, if any, and Δn_{SA} is the change of effective local RI due to specific adsorption. The second optical fiber, the reference fiber sensor without immobilization of a specific recognition molecule, will only measure the thermal and bulk-composition effects and nonspecific binding, if any, and the sensor response can be described by the following relationship:

$$\frac{\Delta I_R}{I_{R0}} = m_R \times (\Delta n_M + \Delta n_{NA}) \quad (2)$$

where $\Delta I_R/I_{R0}$ is the normalized response of the reference fiber and m_R is the calibration slope of the reference fiber.

Rearranging Eq. (1), the sensor response due to specific adsorption only is:

$$\frac{\Delta I_{S,SA}}{I_{S0}} = m_S \times \Delta n_{SA} = \frac{\Delta I_S}{I_{S0}} - m_S \times (\Delta n_M + \Delta n_{NA}) \quad (3)$$

Ideally, if $m_S = m_R$, from Eq. (2) and (3),

$$\frac{\Delta I_{S,SA}}{I_{S0}} = m_S \times \Delta n_{SA} = \frac{\Delta I_S}{I_{S0}} - \frac{\Delta I_R}{I_{R0}} \quad (4)$$

In case $m_S \neq m_R$, i.e., the surface coverages of the AuNPs on the analysis and reference fibers are not exactly the same, from Eqs. (2) and (3),

$$\frac{\Delta I_{S,SA}}{I_{S0}} = \frac{\Delta I_S}{I_{S0}} - \frac{m_S}{m_R} \times \frac{\Delta I_R}{I_{R0}} \quad (5)$$

When the injection of a sample causes a change of medium RI, Δn_M, the normalized responses of the analysis and reference fibers will be $\Delta I_{S,M}/I_{S0}$ and $\Delta I_{R,M}/I_{R0}$, respectively. Both these changes can be easily interrogated from the sensorgrams, as illustrated by Fig. 3A. As plots of $\Delta I_{S,M}/I_{S0}$ and $\Delta I_{R,M}/I_{R0}$ versus Δn_M represent the calibration slopes of the analysis and reference fibers, respectively, Eq. (5) can be rewritten as:

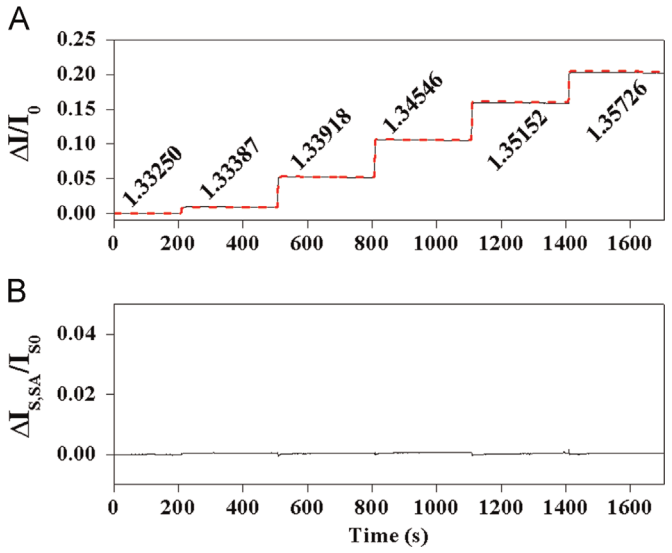

Fig. 3. (A) Real-time normalized responses of an analysis fiber (black solid line) and a reference fiber (red dash line) upon sequential injection of PBS samples at increasing refractive index (1.33387–1.35726). (B) Compensated response obtained by the self-referencing sensing system for the data in A. (For interpretation of the references to color in this figure legend, the reader is referred to the web version of this article.)

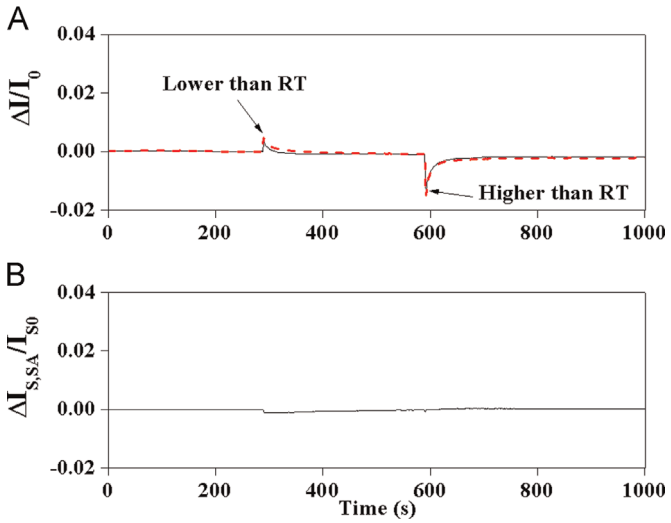

Fig. 4. (A) Real-time normalized responses of an analysis fiber (black solid line) and a reference fiber (red dash line) in water in response to injection of ultrapure water samples at about 15 °C and 45 °C. (B) Compensated response obtained by the self-referencing sensing system in response to temperature changes as above. (For interpretation of the references to color in this figure legend, the reader is referred to the web version of this article.)

$$\frac{\Delta I_{S,SA}}{I_{S0}} = \frac{\Delta I_S}{I_{S0}} - \frac{\Delta I_{S,M}/I_{S0}}{\Delta I_{R,M}/I_{R0}} \times \frac{\Delta I_R}{I_{R0}} \quad (6)$$

This is an interesting result implying that the intentional use of a blank and a sample with different RI values will allow an easy and more accurate compensation of thermal and bulk-composition effects as well as nonspecific adsorption, even if the surface coverages of AuNPs on the two fibers are not exactly the same.

3.2. Compensation for bulk refractive index effect

To quantify the sensor responses of the self-referencing FOPPR sensing system to bulk RI variations, ultrapure water and PBS solutions with different refractive indexes (1.33250–1.35726) were successively injected into a sensor chip. Representative sensorgrams of the normalized responses of both the analysis and reference fibers are shown in Fig. 3A. The baselines were established as both fibers were in contact with ultrapure water. From the baseline of the analysis fiber without and with self-referencing, the power stability or the relative standard deviation of the noises (σ) are estimated to be 0.0073% (SNR = $20 \times \log(1/0.000073)$ = 83 dB) and 0.0048% (SNR = 86 dB) per 120 s, respectively [27,28]. Both SNR values are below the maximum SNR of the analog to digital converter. Including the noises due to five injections of ultrapure water samples, the sum of squared residuals (SSE) about regression of the normalized response of the analysis fiber is estimated to be 0.0319%. With the stepwise increase of RI of the injected samples, the normalized responses of both fibers show step-up trends. Through correction by Eq. (5), the compensated response ideally should be a straight line with a mean of about zero. As shown in Fig. 3B, the SSE about regression of the compensated response is estimated to be 0.0151%. The comparable and even better SSE values indicate that the self-referencing FOPPR sensing system effectively compensate background RI variations.

3.3. Compensation for temperature effect

In general, the refractive index of a solution relates to temperature. It has been found that a change in temperature causes a change in the RI of water by about 9×10^{-5} RIU °C^{-1} at a wavelength of 632.8 nm [33]. As a result, the pattern of the FOPPR sensor response will follow the temperature variation of a sample, as illustrated in Fig. 4A. In this experiment, the baselines were established as both fibers were in contact with ultrapure water at room temperature. Then ultrapure water samples at about 15 °C and 45 °C were sequentially injected into the sensor chip. In the self-referencing FOPPR sensing system, when temperature decreases, the normalized responses of both fibers rise at the same time; while when temperature increases, the normalized responses of both fibers fall at the same time. From the data shown in Fig. 4A, the SSE about regression of the normalized response of the analysis fiber to include the temperature effect is estimated to be 0.2316%. By Eq. (5), the pair-wise differences of normalized responses between fibers are plotted versus time as shown in Fig. 4B, and the SSE about regression of the compensated response is estimated to be 0.0284%. Such a result indicates that the self-referencing FOPPR sensing system provides excellent compensation for temperature variation. On the other hand, compensation of temperature change in SPR sensors is challenging [6,7].

3.4. Compensation for nonspecific adsorption effect

For biosensor application in real samples, nonspecific adsorption will lead to error in biosensors based on detection of RI change near the biosensor surface. Although various approaches have been employed to minimize nonspecific adsorption at sensor surfaces [34–37], it is still technology challenging to completely eliminate this effect. An alternative is through compensation of nonspecific adsorption effect by a reference sensor. If the reference sensor is identical except without a functionalized recognition molecule, the reference sensor can be used to compensate for nonspecific adsorption. Fig. 5A shows the data for both the analysis and reference fibers during sequential exposure of both fibers to various samples of anti-biotin dissolved in PBS buffer with increasing concentration from 26.2 nM to 349 nM. There is a little nonspecific adsorption on the reference fiber while the analysis fiber yields larger signals. By Eq. (4), the compensated response is calculated via the pair-wise differences of normalized responses between fibers and then plotted versus time as shown in Fig. 5B. The calibration graph of $\Delta I_{S,SA}/I_{S0}$ versus log anti-biotin concentration can be seen from Fig. 5E (black

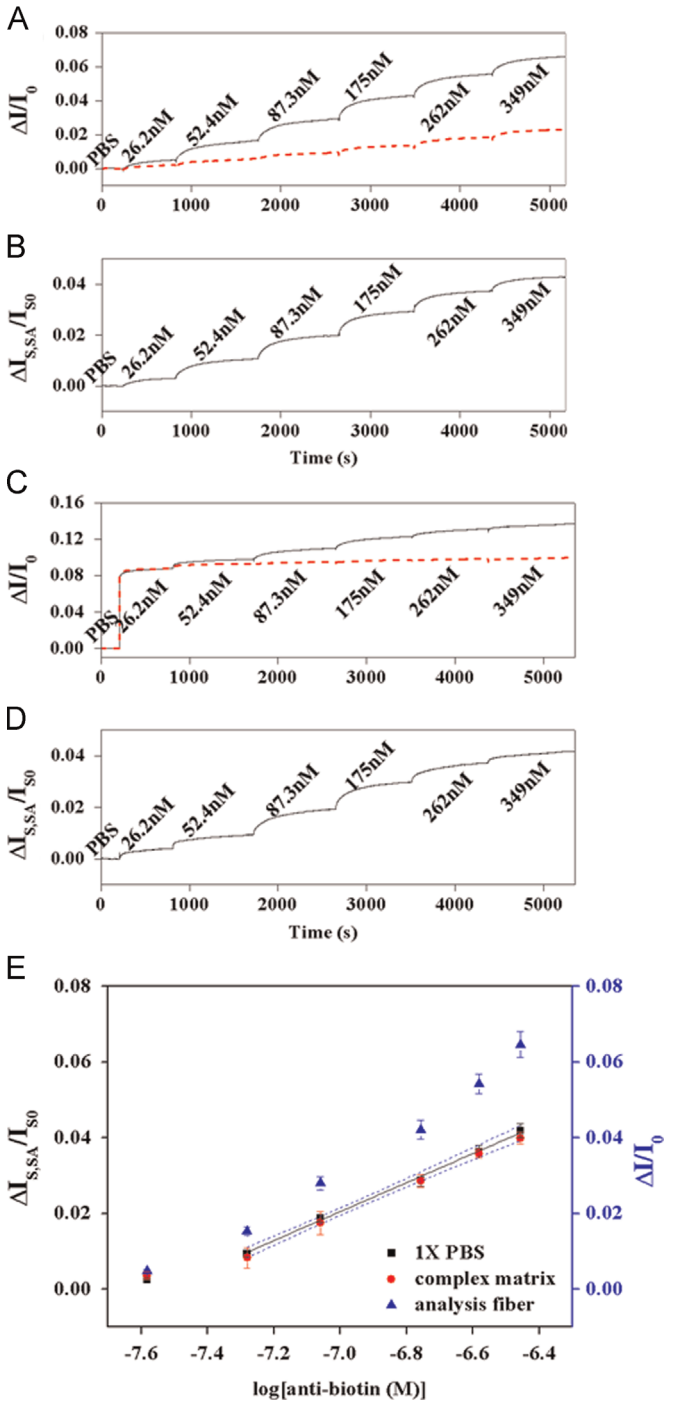

Fig. 5. Real-time normalized responses of an analysis fiber (black solid line) and a reference fiber (red dash line) upon sequential injection of samples with increasing concentration (26.2–349 nM) of anti-biotin in (A) 1X PBS and (C) 10X PBS containing erythrosine (4×10^{-5} g/mL). Compensated response obtained by the self-referencing sensing system for (B) the data in A and (D) the data in C. (E) Calibration graphs of anti-biotin obtained by the self-referencing sensing system in 1X PBS (black square) and in complex matrix (red circle) over the concentration range of 52.4–349 nM, and that by the analysis fiber only in 1X PBS (blue triangle). The blue dash lines represent the 95% confidence interval for the calibration graph of anti-biotin in 1X PBS by the self-referencing sensing system. (For interpretation of the references to color in this figure legend, the reader is referred to the web version of this article.)

square), which is linear in the concentration range between 52.4 nM and 349 nM (correlation coefficient, $r=0.9989$, $n=3$). The limit of detection (LOD) of the self-referencing FOPPR sensing system for anti-biotin is estimated to be 29.5 nM. On the other hand, if only the

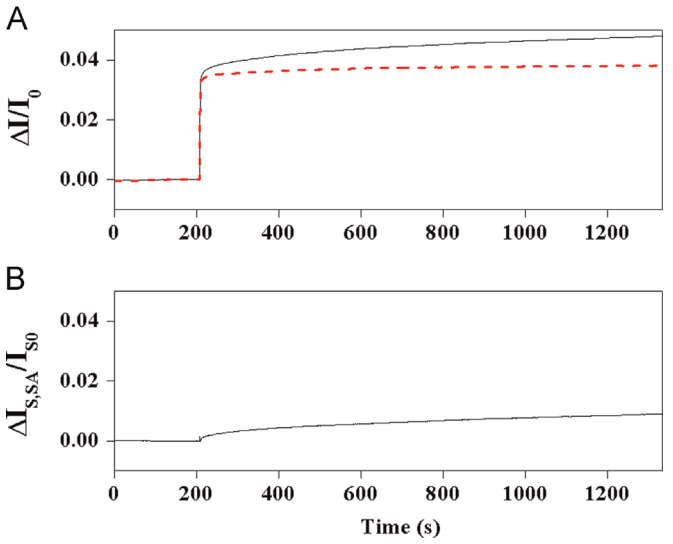

Fig. 6. (A) Real-time normalized responses of an analysis fiber (black solid line) and a reference fiber (red dash line) upon injection of an anti-biotin sample with a concentration of 52.4 nM in 5X PBS (RI=1.33918). (B) Compensated response obtained by the self-referencing sensing system for the data in A. (For interpretation of the references to color in this figure legend, the reader is referred to the web version of this article.)

normalized response from the analysis fiber is used to establish the calibration graph as shown in Fig. 5E (blue triangle), the error could be at least 46%.

3.5. Compensation for both bulk refractive index and nonspecific adsorption effects

In this study, the analysis and reference fiber sensors with a small difference in calibration slopes were intentionally selected in order to demonstrate the feasibility of using Eq. (5) in self-referencing even if the calibration slopes are not exactly the same. Here, the RIs of the buffers used to establish the baselines and to dissolve the samples were chosen to be different in order to estimate $\Delta I_{S,M}/I_{S0}$ and $\Delta I_{R,M}/I_{R0}$ by taking advantage of the sharp responses to RI change by the two fiber sensors. As shown in Fig. 6A, after the baselines had been established using a 1X PBS buffer (RI=1.33387), a solution of anti-biotin (52.4 nM) spiked in 5X PBS (RI=1.33918) was injected into the sensor chip. The normalized responses of both the analysis fiber and reference fiber increase immediately and simultaneously due to the increase in RI. Then the normalized response of the analysis fiber continues to increase and follow a molecular binding kinetic curve [21] while the normalized response of the reference fiber increases very slowly due to nonspecific adsorption. The normalized responses due to matrix change, $\Delta I_{S,M}/I_{S0}$ and $\Delta I_{R,M}/I_{R0}$ can be easily determined by estimation of $\Delta I_{S,M}$ and $\Delta I_{R,M}$ using the intersection points of the molecular binding kinetic curve and the response curve due to bulk RI change. As the regions of sharp rise in normalized responses provide a mechanism to correct for the difference in calibration slopes between the analysis and reference fibers, the compensated response as shown in Fig. 6B can be calculated by Eq. (5). From the calibration graph as shown in Fig. 5E, the concentration of anti-biotin in the spiked sample was estimated to be 54.1 ± 4.0 nM ($n=3$), yielding a percent recovery of 103.2%. Such a result indicates that the self-referencing FOPPR sensing system provides excellent compensation for both the bulk refractive index effect and the nonspecific adsorption effect in a sample.

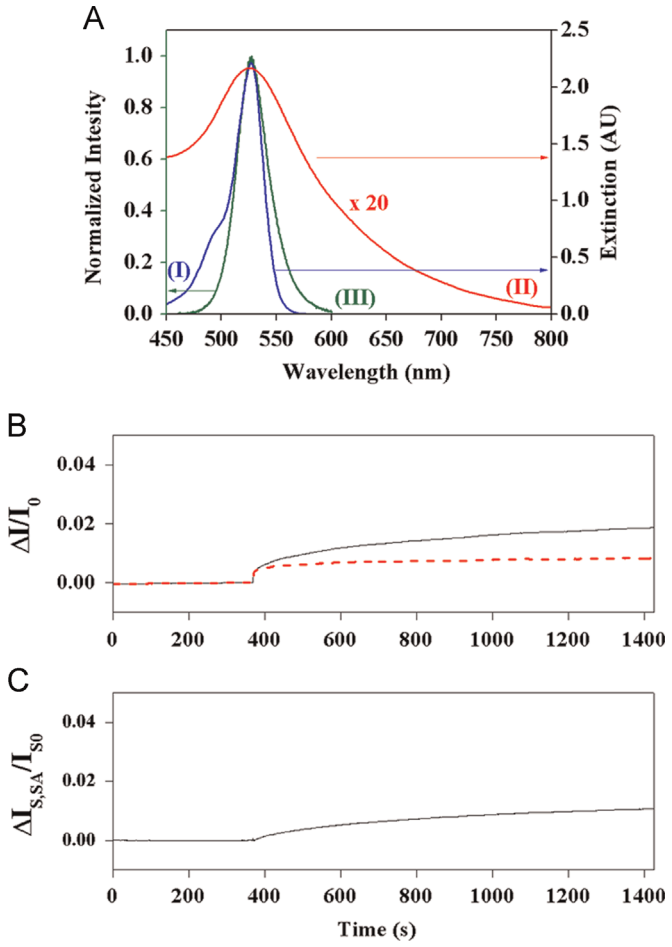

Fig. 7. (A) Extinction spectra of (I) an erythrosine solution (blue line) and (II) an AuNP layer on the core surface of an optical fiber obtained by in-line transmission (red line, the extinction was multiplied by 20 times to aid the eyes), and (III) emission spectrum of the LED (green line). (B) Real-time normalized responses of an analysis fiber (black solid line) and a reference fiber (red dash line) upon injection of an anti-biotin sample with a concentration of 52.4 nM in erythrosine solution. (C) Compensated response obtained by the self-referencing sensing system for the data in B. (For interpretation of the references to color in this figure legend, the reader is referred to the web version of this article.)

3.6. Compensation for color interference

When a real sample has a color overlapping with the excitation spectrum of the incident light, the evanescent wave at the fiber core surface may be absorbed by the matrix of the real sample as well as by the AuNPs [5]. Consequently, spectral interference will occur and lead to error in the analysis. In this study, we artificially made a color matrix by adding a dye, erythrosine, in the sample. The spectrum of erythrosine (Curve I, blue line) is shown in Fig. 7A. Obviously, as shown in Fig. 7A, the plasmon absorption band of the AuNP layer (Curve II, red line) is overlapping with the emission band of the LED (Curve III, green line), and the peak wavelength of a solution of erythrosine (2×10^{-5} g/mL) at about 527 nm is also overlapping with the emission band of the LED (Curve III, green line). Fig. 7B shows that the normalized responses of both the analysis and the reference fibers increase immediately and simultaneously due to the color interference when an erythrosine solution spiked with anti-biotin (52.4 nM) was injected into the sensor chip. After the sharp rise in signals, the normalized responses of both the analysis and the reference fibers follow similar patterns as described in Section 3.5 above. By the same rationale, the compensated sensor response as shown in Fig. 7C can be calculated by Eq. (5). From the calibration graph as shown in Fig. 5E, the concentration of anti-biotin in the spiked sample was estimated to be 49.2 ± 5.2 nM ($n=3$), yielding a percent recovery of 93.9%. Such a result indicates that the self-referencing FOPPR sensing system provides excellent compensation for color interference in the sample matrix.

3.7. Direct detection of anti-biotin in complex medium

Many kinds of real samples, such as whole blood and plant saps, have very complex matrixes that will bias the results of direct biosensing in terms of RI difference between sample and blank, color interference, and nonspecific adsorption. In this study, we used a mimic complex sample composing of a high RI buffer and erythrosine as a color interfering substance to demonstrate the feasibility of the self-referencing FOPPR sensing system for direct detection of anti-biotin in such a complex sample. As shown in Fig. 5C, a 1X PBS solution was injected into a sensor chip to establish flat baselines, and then various samples of erythrosine (4×10^{-5} g/mL) dissolved in 10X PBS buffer and spiked with increasing concentration of anti-biotin from 26.2 nM to 349 nM were sequentially injected into the sensor chip. The normalized responses of both the analysis and the reference fibers follow similar patterns as described in Section 3.5 above. By Eq. (5), the compensated sensor response $\Delta I_{S,SA}/I_{S0}$ is plotted versus time as shown in Fig. 5D. From the calibration graph of $\Delta I_{S,SA}/I_{S0}$ versus log anti-biotin concentration as shown in Fig. 5E, the plot has a linear relationship ($r=0.9993$, $n=3$) over the concentration range between 52.4 nM and 349 nM. The LOD of the self-referencing FOPPR sensing system for anti-biotin in such a complex medium was 31.8 nM, which is similar to that in 1X PBS (LOD=29.5 nM). To compare the results from samples in simple buffer and in complex matrix, statistical analysis of the results from these two groups was performed by pair-t test (GraphPad InStat) to determine whether the mean of the differences between the two groups differs significantly from zero. The two-sided p value was 0.1933 and the t value with 14° of freedom was 1.367, suggesting that the mean of the differences between the two groups is not considered significant at the 95% confidence interval. The mean difference was 0.001018 as compared to the respective standard errors of 0.003141 and 0.003162 in the two groups, indicating the results from each group agree with each other at the 95% confidence interval. These results show that the self-referencing FOPPR sensing system can provide an easy, rapid, and high sensitivity method to detect analyte in complex samples.

4. Conclusions

We have demonstrated a new approach to plasmon resonance biosensing based on a self-referencing dual-channel FOPPR sensing system. This approach allows the use of a reference fiber for accurate compensation of systematic errors, such as temperature fluctuation, bulk refractive index change, color interference, and/or nonspecific adsorption, of the analysis fiber in a single microfluidic chip. The self-referencing mechanism would allow real-time plasmon resonance biosensing applications outside the laboratory where room temperature conditions cannot be held constant. It is also particularly useful for biosensing in complex real samples, in which interfering effects pose a great challenge for many label-free refractive-index-based biosensors. Since the FOPPR sensor is based on normalized response for data analysis, the need for precise optical alignment is alleviated. Hence, together with self-referencing mechanism for compensation of thermal and bulk-composition effects as well as nonspecific adsorption, the dual-channel FOPPR sensing system has potential advantages to be developed as a portable biosensor for on-site chemical and biochemical analysis in the fields of environment, agriculture, food, and healthcare.

Acknowledgments

This study is supported by the Ministry of Science and Technology of Taiwan (NSC95-3114-P-194-001-MY3 and MOST103-2120-M-194-004-CC2). Helpful discussion with Prof. Sung-Nien Yu is acknowledged.

References

[1] X. Fan, I.M. White, S.I. Shopova, H. Zhu, J.D. Suter, Y. Sun, Sensitive optical biosensors for unlabeled targets: a review, Anal. Chim. Acta 620 (2008) 8–26.
[2] J. Homola, Surface plasmon resonance sensors for detection of chemical and biological species, Chem. Rev. 108 (2008) 462–493.
[3] K.M. Mayer, J.H. Hafner, Localized surface plasmon resonance sensors, Chem. Rev. 111 (2011) 3828–3857.
[4] L.L. Chan, B.T. Cunningham, P.Y. Li, D. Puff, A self-referencing method for microplate label-free photonic-crystal biosensors, IEEE Sens. J. 6 (2006) 1551–1556.
[5] H.-Y. Lin, C.-H. Huang, S.-H. Lu, I.-T. Kuo, L.-K. Chau, Direct detection of orchid viruses using nanorod-based fiber optic particle plasmon resonance immunosensor, Biosens. Bioelectron. 51 (2014) 371–378.
[6] A.N. Naimushin, S.D. Soelberg, D.U. Bartholomew, J.L. Elkind, C.E. Furlong, A portable surface plasmon resonance (SPR) sensor system with temperature regulation, Sens. Actuators B 96 (2003) 253–260.
[7] M.J. O'Brien II, S. Brueck, V.H. Perez-Luna, L.M. Tender, G.P. Lopez, SPR biosensors: simultaneously removing thermal and bulk-composition effects, Biosens. Bioelectron. 14 (1999) 145–154.
[8] M.E. Stewart, C.R. Anderton, L.B. Thompson, J. Maria, S.K. Gray, J.A. Rogers, R. G. Nuzzo, Nanostructured plasmonic sensors, Chem. Rev. 108 (2008) 494–521.
[9] J.N. Anker, W.P. Hall, O. Lyandres, N.C. Shah, J. Zhao, R.P. Van Duyne, Biosensing with plasmonic nanosensors, Nat. Mater. 7 (2008) 442–453.
[10] B. Sepúlveda, P.C. Angelomé, L.M. Lechuga, L.M. Liz-Marzán, LSPR-based nanobiosensors, Nano Today 4 (2009) 244–251.
[11] C.-D. Chen, S.-F. Cheng, L.-K. Chau, C.C. Wang, Sensing capability of the localized surface plasmon resonance of gold nanorods, Biosens. Bioelectron. 22 (2007) 926–932.
[12] S.-F. Cheng, L.-K. Chau, K.-C. Pao, Sol–gel-coated poly (methyl methacrylate) as a substrate for localized surface plasmon resonance biosensors, J. Biomed. Nanotechnol. 1 (2005) 143–150.
[13] N. Nath, A. Chilkoti, A colorimetric gold nanoparticle sensor to interrogate biomolecular interactions in real time on a surface, Anal. Chem. 74 (2002) 504–509.
[14] N.-S. Lai, C.-C. Wang, H.-L. Chiang, L.-K. Chau, Detection of antinuclear antibodies by a colloidal gold modified optical fiber: comparison with ELISA, Anal. Bioanal. Chem. 388 (2007) 901–907.
[15] P. Neuzil, J. Reboud, Palm-sized biodetection system based on localized surface plasmon resonance, Anal. Chem. 80 (2008) 6100–6103.
[16] L.-K. Chau, Y.-F. Lin, S.-F. Cheng, T.-J. Lin, Fiber-optic chemical and biochemical probes based on localized surface plasmon resonance, Sens. Actuators B 113 (2006) 100–105.
[17] L.K. Chau, C.W. Kuo, Y.W. Chu, S.H. Liao, Y.T. Lin, C. Wang, A fiber optic particle plasmon resonance biosensing platform based on detection of light scattering intensity from the proximal end, J. Chin. Chem. Soc. 58 (2011) 786–792.
[18] S.-F. Cheng, L.-K. Chau, Colloidal gold-modified optical fiber for chemical and biochemical sensing, Anal. Chem. 75 (2003) 16–21.
[19] C.-Y. Chiang, M.-L. Hsieh, K.-W. Huang, L.-K. Chau, C.-M. Chang, S.-R. Lyu, Fiber-optic particle plasmon resonance sensor for detection of interleukin-1β in synovial fluids, Biosens. Bioelectron. 26 (2010) 1036–1042.
[20] K.-W. Huang, C.-W. Hsieh, H.-C. Kan, M.-L. Hsieh, S. Hsieh, L.-K. Chau, T.-E. Cheng, W.-T. Lin, Improved performance of aminopropylsilatrane over aminopropyltriethoxysilane as a linker for nanoparticle-based plasmon resonance sensors, Sens. Actuators B 163 (2012) 207–215.
[21] T.-C. Chang, C.-C. Wu, S.-C. Wang, L.-K. Chau, W.-H. Hsieh, Using a fiber optic particle plasmon resonance biosensor to determine kinetic constants of antigen–antibody binding reaction, Anal. Chem. 85 (2013) 245–250.
[22] W.-T. Hsu, W.-H. Hsieh, S.-F. Cheng, C.-P. Jen, C.-C. Wu, C.-H. Li, C.-Y. Lee, W.-Y. Li, L.-K. Chau, C.-Y. Chiang, Integration of fiber optic-particle plasmon resonance biosensor with microfluidic chip, Anal. Chim. Acta 697 (2011) 75–82.
[23] Y.-C. Huang, C.-Y. Chiang, C.-H. Li, T.-C. Chang, C.-S. Chiang, L.-K. Chau, K.-W. Huang, C.-W. Wu, S.-C. Wang, S.-R. Lyu, Quantification of tumor necrosis factor-α and matrix metalloproteinases-3 in synovial fluid by a fiber-optic particle plasmon resonance sensor, Analyst 138 (2013) 4599–4606.
[24] H.-Y. Lin, C.-H. Huang, C.-C. Huang, Y.-C. Liu, L.-K. Chau, Multiple resonance fiber-optic sensor with time division multiplexing for multianalyte detection, Opt. Lett. 37 (2012) 3969–3971.
[25] Y. Wang, W. Qian, Y. Tan, S. Ding, A label-free biosensor based on gold nanoshell monolayers for monitoring biomolecular interactions in diluted whole blood, Biosens. Bioelectron. 23 (2008) 1166–1170.
[26] C.-H. Chen, B.-K. Yeh, J.-L. Tang, W.-T. Wu, Fabrication quality analysis of a fiber optic refractive index sensor created by CO_2 laser machining, Sensors 13 (2013) 4067–4087.
[27] H.V. Malmstadt, C.G. Enke, S.R. Crouch, Electronic Measurements for Scientists, W. A. Benjamin, Menlo Park (1974), p. 746–749.
[28] V. Mladenov, P. Karampelas, G. Tsenov, V. Vita, Approximation formula for easy calculation of signal-to-noise ratio of sigma-delta modulators, ISRN Signal Process. 2011 (2011) 731989.
[29] F. Payne, Z. Hale, Deviation from Beer's law in multimode optical fibre evanescent field sensors, Int. J. Optoelectron. 8 (1993) 743–748.
[30] L.-K. Chau, C.-Y. Chiang, W.-T. Hsu, S.-H. Chen, S.-F. Cheng, Optical waveguide-based biosensors using noble metal nonoparticles, in: L.-K. Chau, H.-T. Chang (Eds.), From Bioimaging to Biosensors: Noble Metal Nanoparticles in Biodetection, Pan Stanford Publishing Pte. Ltd., Singapore, 2013, pp. 77–102.
[31] X. Liu, M. Atwater, J. Wang, Q. Huo, Extinction coefficient of gold nanoparticles with different sizes and different capping ligands, Colloids Surf. B 58 (2007) 3–7.
[32] N.J. Harrick, Internal Reflection, Wiley, New York (1967), p. 30–33.
[33] P. Schiebener, J. Straub, J.L. Sengers, J. Gallagher, Refractive index of water and steam as function of wavelength, temperature and density, J. Phys. Chem. Ref. Data 19 (1990) 677–717.
[34] X. Qian, S.J. Metallo, I.S. Choi, H. Wu, M.N. Liang, G.M. Whitesides, Arrays of self-assembled monolayers for studying inhibition of bacterial adhesion, Anal. Chem. 74 (2002) 1805–1810.
[35] O.R. Bolduc, J.-F. Masson, Monolayers of 3-mercaptopropyl-amino acid to reduce the nonspecific adsorption of serum proteins on the surface of biosensors, Langmuir 24 (2008) 12085–12091.
[36] Z. Zhang, M. Zhang, S. Chen, T.A. Horbett, B.D. Ratner, S. Jiang, Blood compatibility of surfaces with superlow protein adsorption, Biomaterials 29 (2008) 4285–4291.
[37] K.P. García, K. Zarschler, L. Barbaro, J.A. Barreto, W. O'Malley, L. Spiccia, H. Stephan, B. Graham, Zwitterionic-coated "Stealth" nanoparticles for biomedical applications: recent advances in countering biomolecular corona formation and uptake by the mononuclear phagocyte system, Small 10 (2014) 2516–2529.